2005 IEEE Vehicle Power and Propulsion Conference, October 2005, pp. 819-830.

Topologies for Future Automotive Generators – Part I: Modeling and Analytics

L. M. Lorilla, *Student member, IEEE,* T. A. Keim, *Member, IEEE,*
J. H. Lang, *Member, IEEE,* D. J. Perreault, *Member, IEEE*

***Abstract*— This paper compares the relative suitability of four different alternator topologies for use in an advanced automobile electrical system. The four candidate topologies are: the salient- and non-salient-pole wound-field synchronous alternators, the Lundell alternator, and the homopolar inductor alternator. The analysis is made with the alternator utilizing a switched-mode rectifier that enables load matching for optimal power transmission. Part I models and compares the alternators using hand calculations. Lumped parameter models of each of the four alternators are derived. The output power and efficiency of each machine is evaluated when utilized with a switched-mode boost rectifier and operating at the load matched condition. A direct mathematical comparison of the sizing equations for the four classes of machines is offered. Based on the analysis, the Lundell alternator has the highest power output and efficiency when compared at the same dimensions and field ampere turns excitation. Part II will cover a more detailed and accurate cost optimization of the four alternators while subject to the constraints and requirements of future automobiles.**

***Index Terms*-- Automotive alternator, synchronous generator, switched-mode rectifier, non-salient wound-field alternator, salient wound-field alternator, Lundell alternator, homopolar inductor alternator , constant voltage load, generator lumped parameters**

I. NOMENCLATURE

a	number of parallel windings
b_p	pole width
b_{pN}	pole width of north pole at a particular axial location
b_{pS}	pole width of south pole at a particular axial location
B	flux density
B_r	air gap flux density due to the field winding
B_s	air gap flux density due to the armature currents
F_r	MMF due to the field winding
F_s	MMF due to the three phase armature currents
g	air gap width
$g1$	shorter air gap width
$g2$	longer air gap width
i_a, i_b, i_c	armature phase currents
i_f	field current
I_s	magnitude of armature phase current
k_{wf}	field distribution winding factor
k_{wn}	armature distribution winding factor of nth harmonic
L	air gap length
L_{af}	field armature mutual inductance
L_s	synchronous inductance
N_fI_f	field ampere turns
N_s	series armature turns
p	pole pairs
P	output power
R	equivalent resistance due to effects of diode rectifer
R_s	armature series resistance
r_a	physical armature resistance
V_d	diode drop
V_o	effective voltage at output of rectifier
V_{sa}, V_{sb}, V_{sc}	back-emf voltages
X_d, X_q	direct and quadrature reactances
z	axial location
b	pole width over pole pair pitch
b'	pole width over pole pitch (pole fraction)
d	electrical angle when t=0
h	efficiency
L	permeance per unit area
l	flux linked
l_{af}	flux linked by armature winding due to field current
l_{as}	flux linked by armature winding due to three phase armature currents
ω	electrical frequency in rad/s
θ_r	rotor angle in mechanical degrees
τ_p	pole pitch

II. INTRODUCTION

It is commonly asserted that the Lundell (or claw pole) alternator construction that is universally used on modern automobiles will need to be replaced to meet the increased power demands of future vehicles. Nevertheless, a design strategy has been introduced that uses switched-mode rectification to substantially enhance the Lundell alternator/rectifier system [1]. This approach allows the effective voltage seen by the bridge rectifier to be varied in what is effectively a load-impedance matching technique to enable optimum transmission of power. The use of this technique with an over-the-counter automotive alternator has shown substantial increases in power output and efficiency. One goal of the study described here is to determine how much more performance can be obtained if the Lundell alternator is optimized for use with the switched mode rectifier. In other words, how much more cost effective will the alternator be having been reoptimized for the new duty? Conclusions are

This work was fully supported by the MIT/Industry Consortium on Advanced Electrical/Electronic Components and Systems.

also offered concerning the feasibility of building belt-driven automotive alternators for future high-electric-demand automobiles.

In addition to the Lundell alternator [2,3], alternative alternator designs are investigated and compared, including the wound-field synchronous alternator and the homopolar inductor alternator [4,5,6,7,8]. All candidate alternators are required to produce a minimum specified power at each of two speeds, and to operate at and achieve a minimum efficiency at a third combination of speed and load. The machines are constrained to obey heat flux limitations based on heat flux levels obtained in today's automotive alternators. Magnetic parts are sized to avoid magnetic saturation. The resulting rotor inertias and rotational stresses are evaluated and compared.

III. Alternator Types

Figures 1 through 4 present the alternative alternator constructions under consideration. These diagrams are somewhat stylized representations which can be useful for comparing specific machines. These figures are generated by a drawing program from a few specific parameters. The diagrams to the left reasonably portray a section view in the axial direction, assuming that the section is taken at the boundary between the motor stack and the end turns. Many of the dimensions of the drawing represent values determined during the course of the cost optimization. (Figures 1 through 4 merely introduce the machine types; the dimensions in these figures do not represent optimized machines.) In an optimized machine, the rotor outside diameter, stator inside and outside diameter are to scale. So are the stator and (if applicable) the rotor slot depth and slot fraction. The inner circle does not represent an optimized value. The diagrams to the right of each motor axial section represent another rotor section, this time a vertical section taken through the diameter. In the representation of an optimized machine, all the axial dimensions represent values selected by the optimization process. The small blocks extending from the blocks representing the stator (and possibly rotor) stack(s) are approximations of the volume occupied by winding end turns.

The first class of alternators is the wound-field synchronous alternator, of which we have the non-salient and salient-pole types shown in Figures 1 and 2, respectively. The non-salient-pole wound-field alternator has the field winding wound in slots such that the resulting flux density is approximately sinusoidal. The salient-pole wound-field alternator has the field winding wound around poles. Consecutive poles are wound to have opposite polarities.

The third machine is the Lundell or claw-pole alternator which is currently used in automobiles (Fig. 3). The Lundell alternator has cantilevered poles. All north poles are attached to a disk on one side, and all south poles are attached to a disk on the opposite side. The poles alternate polarities as one traverses the air gap in the circumferential direction. The field winding is a single coil wound concentric with the axis of rotation.

The fourth type of machine is the homopolar inductor alternator shown in Fig. 4. This machine has a field winding wound on the stator concentric with the axis of rotation. It is wound right next to the armature winding in the stator. The machine has two axially distinct stator stacks, and excitation flux flows in a path that crosses one air gap in a radially outward direction, continues axially through a tubular ferromagnetic path (the outermost member in Fig. 4) to the other stator stack, crosses the air gap at the second stack in the radially inward direction, and returns axially through the rotor body. The north poles are all formed from the rotor body at the axial location of one of the stacks. The south poles are formed on the same rotor body at a different axial location. All four alternators have conventional three-phase armature windings wound along slots in the stator.

Fig. 1. Non-salient pole wound-field synchronous alternator

Fig. 2. Salient-pole wound-field synchronous alternator

Fig. 3. Lundell alternator

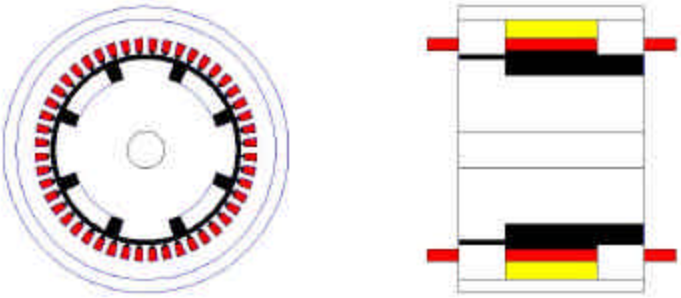

Fig. 4. Homopolar inductor alternator

Research has previously been done on all four alternators. The rotor construction of the wound field non-salient pole synchronous alternator is more robust than the salient pole version because its field windings are located in the rotor slots. It can therefore be run at higher speeds than the salient-pole rotor . The salient pole synchronous generator has the highest electrical output per pound per rpm among all generators according to a NASA study published in 1965 [9]. It also has the lowest reactances and therefore its regulation and transient performance are the best. Its speed limitations are due to the high stresses that result from centrifugal loading of the field coils . For extreme environments, the Lundell and homopolar inductor alternator are more likely to be used than the wound-field alternators . The Lundell is typically smaller and lighter than the homopolar inductor alternator [9]. The Lundell, however, is more stress limited because of its cantilevered poles [10]. On the other hand, due to its robust rotor structure, the homopolar inductor alternator can be run at the highest speeds among all four alternators [9]. The flux per pole is higher for the homopolar inductor alternator than that of a salient pole alternator because of the DC flux that it has to carry. This DC flux makes it larger than the equivalently rated salient pole alternator [10]. Also, the field excitation coil location increases the length of the machine. It increases the length of the stator conductor where no voltage is being generated thus resulting in higher copper losses [11]. The homopolar inductor alternator is the heaviest of all the alternators at the same rpm [9]. The many interlocked trade-offs among these machine types necessitates careful evaluation and comparison to identify suitable designs for future alternators.

The work presented involves optimizing these alternators given the requirements of future automobiles and evaluating their performances and limitations. The first set of optimizations will be done assuming these alternators are utilized with a diode bridge. The second set of optimizations will assume that these alternators are connected to a switched mode rectifier. We will then assess how much smaller and less expensive these alternators could be made given the availability of the switched-mode rectifier. This has not been done previously.

IV. Equivalent Circuit model

In order to determine alternator output power, an equivalent electrical circuit model per phase is derived taking saliency into account. This circuit as seen from the terminals of each phase will be a voltage source in series with an inductor and resistor. This circuit successfully models all four alternators.

The flux linkage equations for each alternator can be expressed as

$$\begin{bmatrix} l_a \\ l_b \\ l_c \\ l_f \end{bmatrix} = \begin{bmatrix} L_{s0}+L_{s2}\cos(2pq) & -L_{ss}+L_{s2}\cos(2pq-2p/3) & -L_{ss}+L_{s2}\cos(2pq+2p/3) & M\cos(pq) \\ -L_{ss}+L_{s2}\cos(2pq-2p/3) & L_{s0}+L_{s2}\cos(2pq+2p/3) & -L_{ss}+L_{s2}\cos(2pq) & M\cos(pq-2p/3) \\ -L_{ss}+L_{s2}\cos(2pq+2p/3) & -L_{ss}+L_{s2}\cos(2pq) & L_{s0}+L_{s2}\cos(2pq-2p/3) & M\cos(pq+2p/3) \\ M\cos(pq) & M\cos(pq-2p/3) & M\cos(pq+2p/3) & L_r \end{bmatrix} \begin{bmatrix} i_a \\ i_b \\ i_c \\ i_f \end{bmatrix} \tag{1}$$

where $pq = wt + d$ is in electrical degrees, and the L_{s2} term reflects saliency. The flux linked by the armature winding due to the field excitation is

$$l_{af} = M\cos(pq)i_f \tag{2}$$

The generated back voltage is

$$\frac{dl_{af}}{dt} = -wM\sin(pq)if \tag{3}$$

The three-phase armature currents (motor convention) may be expressed as

$$i_a = I_s\sin(pq-f) \tag{4}$$

$$i_b = I_s\sin(pq-f-2p/3) \tag{5}$$

$$i_c = I_s\sin(pq-f+2p/3) \tag{6}$$

where f is the internal power factor angle or the angle between the back-emf and the armature phase current. The flux linked by phase a due to all three armature phases (with i_f equal to zero) is

$$\begin{aligned} l_{as} &= (L_{s0}+L_{s2}\cos(2pq))I_s\sin(pq-f) \\ &\quad +(-L_{ss}+L_{s2}\cos(2pq-2p/3))I_s\sin(pq-f-2p/3) \\ &\quad +(-L_{ss}+L_{s2}\cos(2pq+2p/3))I_s\sin(pq-f+2p/3) \\ &= (L_{s0}+L_{ss})I_s\sin(pq-f)-\frac{3}{2}L_{s2}I_s\sin((pq-f)+2f) \\ &= (L_{s0}+L_{ss}-\frac{3}{2}L_{s2}\cos(2f))I_s\sin(pq-f) \\ &\quad -\frac{3}{2}L_{s2}\sin(2f)I_s\cos(pq-f) \end{aligned} \tag{7}$$

The non-ohmic voltage drop across phase a due to balanced currents in the three phases is

$$\begin{aligned} \frac{dl_{as}}{dt} &= (L_{s0}+L_{ss}-\frac{3}{2}L_{s2}\cos(2f))\frac{di_a}{dt} \\ &\quad +\frac{3}{2}wL_{s2}\sin(2f)i_a \end{aligned} \tag{8}$$

from which expressions for the equivalent inductance and resistance are

$$L_s = L_{s0}+L_{ss}-\frac{3}{2}L_{s2}\cos(2f) \tag{9}$$

$$R_s = r_a+\frac{3}{2}wL_{s2}\sin(2f) \tag{10}$$

where r_a is the ohmic resistance of the armature winding.

The equivalent circuit representing these equations is shown in Fig. 5. Here V_{sa}, V_{sb}, and V_{sc} are the back-emf excitation voltages, dl_{af}/dt, dl_{bf}/dt, and dl_{cf}/dt.

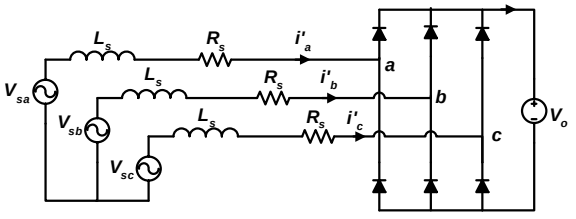

Fig. 5. Alternator, rectifier and constant voltage load circuit

In [1], it is shown that the use of a boost rectifier circuit can be understood as affecting the operation of the machine in essentially the same manner as the circuit of Fig. 5, with the additional feature that varying the duty ratio on the boost switches gives the flexibility to vary the effective dc voltage seen at the rectifier output over a range from zero to the physical limit of the dc source. This boost rectifier (switched-mode rectifier) circuit is shown in Fig. 6.

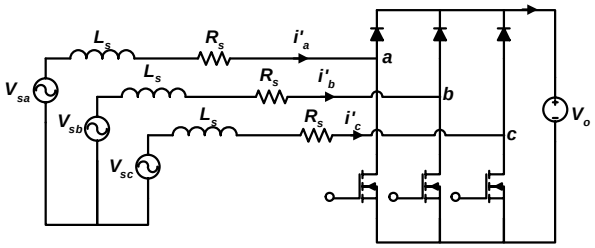

Fig. 6. Alternator, switched-mode rectifier, and constant voltage load circuit

The work above shows how we can conveniently include the effect of rotor saliency in our analysis, but the rectifier in Fig. 5 (or 6) still presents a non-linear element which precludes a fast, analytic solution. Reference [12] provides a convenient approximation which permits a simple solution. Based on [12], the circuit in Fig. 5 (or 6) can be approximated by the circuit shown in Fig. 7 with balanced resistive loads.

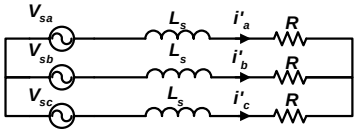

Fig. 7. Equivalent circuit with balanced resistive loads

Following [12], each resistive load has the value

$$R = R_s + \frac{V_{o1}^2 R_s + V_{o1}\sqrt{(wL_s)^2 (V_s^2 - V_{o1}^2) + R_s^2 V_s^2}}{V_s^2 - V_{o1}^2} \qquad (11)$$

where

$$V_{o1} = \frac{4}{p}\left(\frac{V_o}{2} + V_d\right) \qquad (12)$$

and V_d is a diode drop. The power angle can be obtained using

$$\tan(f) = \frac{wL_S}{R} \qquad (13)$$

The output power is then

$$P = \frac{3}{p} I_s V_o = \frac{3}{p}\left(\frac{V_s}{\sqrt{(wL_s)^2 + R^2}}\right) V_o \qquad (14)$$

V. Lumped Parameter Model Derivations

Having completed the circuit model, the appropriate inductances and resistances must then be determined. The procedure is to first determine the flux density in the air gap due to the field winding and the armature windings and then to determine the flux linked by the stator windings from the various sources. The flux linked by each armature winding due to the field excitation will give the back electromotive force while the flux linked by each armature winding due to all three armature phase currents yields the synchronous reactance and equivalent resistance due to armature reaction. The flux density in the air gap is found by multiplying the magnetomotive force (MMF) across the air gap by the permeance per unit area. The MMF drop across the air gap is obtained assuming that the permeability of steel is infinite which implies that flux lines are assumed to terminate perpendicularly to the steel. The details of the process are instructive and straightforward, but also tedious. They are presented in Appendix A.

VI. Simplified Analytical Evaluation and Calculation

The comparative evaluation performed in this paper is conducted in several ways and at several different levels of analytical and computational sophistication. The most extensive comparison is the result of a cost optimization study. This study compares machines of different constructions, each of which is capable of operating over a specified area in power-speed space and meeting certain other constraints. The lowest cost machine of each type meeting all the constraints is selected. The results of that comparison will be presented later in Section VII. In this section we present simplified analytical results which provide some level of insight about how fundamental differences among the machine types give rise to substantial differences in performance.

Consider the approximate equivalent circuit of Fig. 7. It is readily shown that for fixed values of machine parameters, maximum power is delivered to the load at the load-matched condition (when the synchronous reactance equals the effective resistance). The principal focus of this paper is the lowest cost machine meeting a set of specifications. A comparison of machines loaded to maximum power may nevertheless be relevant, because least cost machines may be expected to be loaded to maximum power at one or more design points. As an aside, there is one more consideration to make before accepting that impedance-matched (maximum power) operation is relevant to the pursuit of least-cost machines. If the power rating of the machine is a continuous-, as opposed to a momentary-, rating, impedance-matched operation is relevant only if the machine is well enough cooled to operate at this loading. As a rule, the inductive contribution to machine reactance is dominant over the resistive component, so armature resistive losses tend to be small compared to load power. In practice, it often is possible to design machines which are adequately cooled when operated at the impedance-matched load.

The power delivered to an impedance-matched load can be written approximately as

$$P_{\max} = \frac{3}{4} w \frac{\left(L_{afm} / N_f \right)^2}{L_s} \left(N_f I_f \right)^2 \qquad (15)$$

This is obtained having ignored the armature resistance, diode drop, the larger air gap in the case of the homopolar inductor alternator, saliency, and the leakage inductances. Following (15) and Appendix A.6, the maximum power capability (at the impedance-matched load) for each of the the four machines is

$$P_{\max} \cong 8 k_{wf}^2 \left(\frac{w m_o R L}{p g} \right) \left(\frac{N_f I_f}{2p} \right)^2 \qquad (16)$$

for the non-salient wound-field alternator,

$$P_{\max} \cong 8 \left(\frac{w m_o R L}{p g} \right) \left(\frac{N_f I_f}{2p} \right)^2 \qquad (17)$$

for the salient wound-field alternator,

$$P_{\max} \cong 8 \left(\frac{w m_o R L}{p g} \right) \left(\frac{N_f I_f}{2} \right)^2 \qquad (18)$$

for the Lundell alternator, and

$$P_{\max} \cong 4 \left(\frac{w m_o R L}{p g} \right) \left(\frac{N_f I_f}{2} \right)^2 \qquad (19)$$

for the homopolar inductor alternator.

The symbols *R*, *L*, and *g* in (16)-(19) correspond to the air gap radius, axial length, and radial width respectively. The ratios of output powers among the machines can be found in Table I.

TABLE I
APPROXIMATE RATIOS OF OUTPUT POWER
(COLUMN OVER ROW)

	Non-salient WFSM	Salient WFSM	Lundell	Homopolar
Non-salient WFSM	1	$1/k_{wf}^2$	p^2/k_{wf}^2	$p^2/(2k_{wf}^2)$
Salient WFSM		1	p^2	$p^2/2$
Lundell			1	½
Homopolar				1

It is evident that the Lundell alternator produces the most power in this comparison, followed by the homopolar inductor alternator, the salient-pole wound field alternator, and lastly, the non-salient pole wound field alternator. The factor of p^2 results from the Lundell and inductor alternators having their field windings exciting all the poles. For these two machines, the required number of field ampere turns is independent of the pole count.

Output power comparisons given the same number of field ampere turns are shown below in Fig. 8. The ordinate is terminal voltage operating with a resistive load, normalized to the no-load voltage. This shows that at the same number of field ampere turns, the Lundell outperforms the rest by a large margin. Fig. 8 is prepared for the case of four pole pairs.

The comparison which gives rise to Fig. 8 required many choices to be able to reduce the mathematical expressions for the capabilities of each machine type to simple expressions with many common terms. Many of these choices were of necessity arbitrary, but we tried in every case to be reasonable. The single most important feature giving rise to the striking comparison in Fig. 8 is the fact that in the Lundell and homopolar machines, each ampere turn of field excitation excites field flux in every pole, while in the wound-field machines, each ampere turn excites flux in only one pole. This difference is made evident by requiring all machine types to have the same number of poles. The output power at each of the peaks corresponds directly to equations 16-19.

It can further be argued that comparison at a constant number of field ampere turns is also unreasonable. It is quite credible that the cost of a field ampere turn for a Lundell alternator as measured by most reasonable means is higher than the cost of a field ampere turn for a wound field machine. However, the fundamental message of Fig. 8 does not depend on the comparison being accurate to 5% or even to 50%. Rather, the principal conclusion from Fig. 8 is that the favorable field excitation path of the Lundell alternator (and to a strong extent, the homopolar inductor alternator) is a powerful advantage over other machine types, in terms of power deliverable from a machine of a given size. For other machine types to prevail in an overall comparison, it will be necessary that these other types exhibit strong advantages in other elements of design not considered here.

Fig. 9 shows a different comparison. Here the machine types are compared at constant field ampere turns per pole. On this basis, the salient pole machine is the equal of the Lundell alternator. In practice, it may not be possible to put so many field ampere turns on a salient-pole structure.

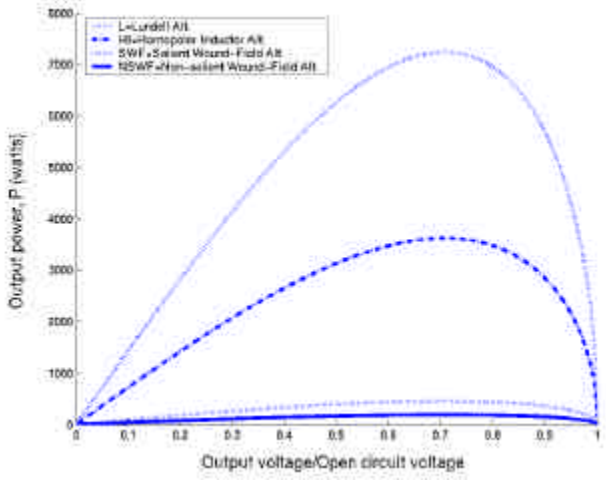

Fig. 8. Output power curves vs. voltage at same number of field ampere turns

At the load matched condition, the alternator efficiency was derived to be

$$h = \frac{wL_s - \dfrac{4R_f L_s^2}{3L_{afm}^2}}{wL_s + R_a} \qquad (20)$$

with a minimum value of zero which occurs when all the power generated is used to power the field winding, resulting in no net output power. Only the field and armature conduction losses were taken into account for this efficiency calculation. The efficiency is independent of field ampere turns and therefore independent of the power requirement. This is because at the load matched condition, the field copper losses and armature losses are proportional to the square of the number of field ampere turns which is the same dependence that the gross output power has on ampere turns as shown in equation 15. The efficiency is also independent of the operating voltage at every load matched point. The efficiency, however, varies with speed. The efficiency increases with larger field armature mutual inductance. Using the same approximations and simplified conditions for the comparison of output power, the Lundell alternator has the highest efficiency. This is primarily due to its large field armature mutual inductance.

Based on these simple calculations, the Lundell alternator is the most promising of the candidates considered here. In addition to its many simplifications, this analysis ignores several other considerations which may substantially influence choice of machine type. For example, for a given diameter and speed, the rotor stresses in a Lundell alternator can be expected to be much higher than in other machine types. If the range of diameters and speeds under consideration are such that rotor stresses are comfortably below stress limits for all machine types, then this difference is unimportant. But if rotor stresses in a Lundell rotor are excessive, the application may require use of a different machine type. But in general, in circumstances where maximum power per unit volume is required and, by implication, assuming comparable average mass densities, also in cases where maximum power per unit weight is the objective, the Lundell machine warrants high consideration.

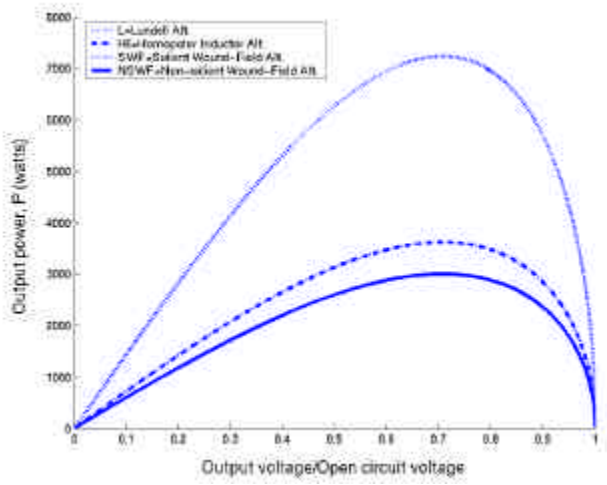

Fig. 9. Output power curves vs. voltage at the same number of field ampere turns per pole

VII. CONCLUSION

To summarize, the lumped parameter models for the four alternators are tied together with the circuit model for the switched-mode rectifier in order to derive analytical expressions for machine performance at the load matched condition. The results indicate the relative performance of the four alternators. The calculations show that the Lundell alternator has the highest output power and efficiency at the load matched condition and is therefore, the preferred candidate for use with the switched-mode rectifier. There are, however, several factors which were ignored in the calculations. These are the mechanical stresses, saturation, heat flux, iron losses, saliency, etc. Therefore, a more accurate study such as a full grid-search optimization taking into account all relevant requirements coupled with finite element analysis of these alternators is worth pursuing. This work is presented in part II.

VIII. APPENDIX

A. Lumped parameter derivations

The appendix provides the detailed derivations of the lumped parameters in Section IV and forms the basis for the evaluation in Section V.

1) General fourier series representation of a rectangular waveform

The Fourier expansion for the flux densities in the air gap can be derived from the generalized rectangular waveform shown in Fig. A.1.

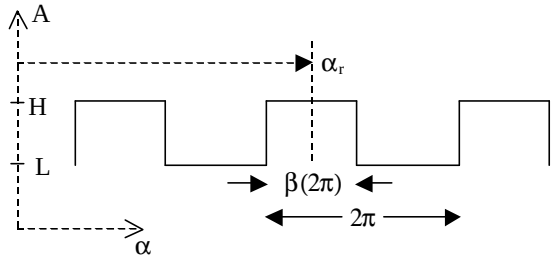

Fig. A.1. Arbitrary rectangular waveform

The waveform could be expressed mathematically as

$$A = \sum_{m=0}^{\infty} A_m \cos(m(a - a_r)) \quad (A.1)$$

$$A_0 = Hb + L(1-b) \quad (A.2)$$

$$A_m = \frac{2}{mp}(H-L)\sin(mbp) \quad (A.3)$$

For a square wave, centered about 0, H=-L and β=1/2. The fourier series coefficients are

$$A_m = \frac{4}{mp} H \sin(mp/2) \quad (A.4)$$

$$A_0 = 0 \quad (A.5)$$

2) Field flux densities

a) Non-salient wound-field alternator field flux density

For the wound-field non-salient pole machine, the step-like MMF is approximated by a square wave whose amplitude is affected by the distribution winding factor. The permeance per unit area is constant at m_0/g or the permeability of free space divided by the air gap width. The MMF distribution can be written as

$$F_r = \sum_{\substack{n=1 \\ n \text{ odd}}}^{\infty} \frac{4}{np} \frac{N_f I_f}{2p} k_{wf} \sin\left(\frac{np}{2}\right) \cos(np(q - q_r)) \quad (A.6)$$

The gap permeance can be defined as

$$\Lambda = \frac{m_0}{g} \quad (A.7)$$

Finally, the air gap flux density due to the field winding can be written as

$$B_r = F_r \Lambda = \left(\sum_{\substack{n=1 \\ n \text{ odd}}}^{\infty} \frac{4}{np} \frac{N_f I_f}{2p} k_{wf} \sin\left(\frac{np}{2}\right) \cos(np(q - q_r)) \right) \frac{m_o}{g} \quad (A.8)$$

where n represents the nth harmonic, p for pole pairs, N_fI_f for field ampere turns, and k_{wf} for the field winding factor. This flux density is shown in Fig. A.2.

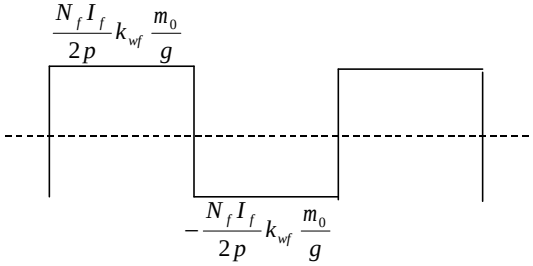

Fig. A.2. Non-salient wound-field alternator flux density waveform

b) Salient-pole wound-field alternator field flux density

The air gap flux density in the salient-pole wound field alternator due to the field winding when expressed as the product of the MMF drop and the permeance per unit area can be expressed as the sum of two waveforms, one due to the north poles and the other due to the south poles. The two waveforms are added together to get the actual flux density shown in Fig. A.3.

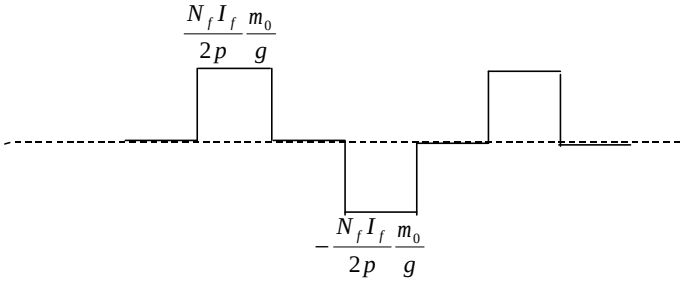

Fig. A.3. Salient wound-field alternator field flux density waveform

The flux density waveform due to the north poles can be expressed as

$$B_{rN} = \sum_{m=0}^{\infty} B_{rNm} \cos(mp(q - q_r)) \quad (A.9)$$

$$B_{rN0} = b\left(\frac{N_f I_f}{2p}\frac{m_0}{g}\right) = \left(\frac{N_f I_f}{2p}\right)\left(b\frac{m_0}{g}\right) = F_{rN}\Lambda_{N0} \quad (A.10)$$

$$B_{rNm} = \frac{2}{mp}\left(\frac{N_f I_f}{2p}\frac{m_0}{g}\right)\sin(mbp) = \left(\frac{N_f I_f}{2p}\right)\left(\frac{2}{mp}\frac{m_0}{g}\sin(mbp)\right) = F_{rN}\Lambda_{Nm} \quad (A.11)$$

where m represents the mth harmonic, and β for the pole width divided by the width of a pole pair. The flux density waveform due to the south poles can be expressed as

$$B_{rS} = \sum_{m=0}^{\infty} B_{rSm} \cos(mp((q - p/p) - q_r)) \quad (A.12)$$

$$B_{rS0} = b\left(-\frac{N_f I_f}{2p}\frac{m_0}{g}\right)=\left(-\frac{N_f I_f}{2p}\right)\left(b\,\frac{m_0}{g}\right)= F_{rS}\Lambda_{S0} \tag{A.13}$$

$$B_{rSm} = \frac{2}{mp}\left(\frac{N_f I_f}{2p}\frac{m_0}{g}\right)\sin(mbp) = \left(-\frac{N_f I_f}{2p}\right)\left(\frac{2}{mp}\frac{m_0}{g}\sin(mbp)\right)= F_{rS}\Lambda_{Sm} \tag{A.14}$$

The sum of the two waveforms give the total flux density waveform in the air gap due to the field winding which can be shown to be

$$B_r = B_{rN} + B_{rS} = \sum_{\substack{m=1\\ m\,\text{odd}}}^{\infty}(B_{rNm} - B_{rSm})\cos(mp(q-q_r))$$

$$B_r = \sum_{\substack{m=1\\ m\,\text{odd}}}^{\infty}(\frac{4}{mp}\frac{N_f I_f}{2p}\frac{m_0}{g}\sin(mbp))\cos(mp(q-q_r)) \tag{A.15}$$

c) Lundell alternator field flux density

Looking at the Lundell alternator, along a slice at some circumferential position, the flux density waveform will look like the waveform shown in Fig. A.4.

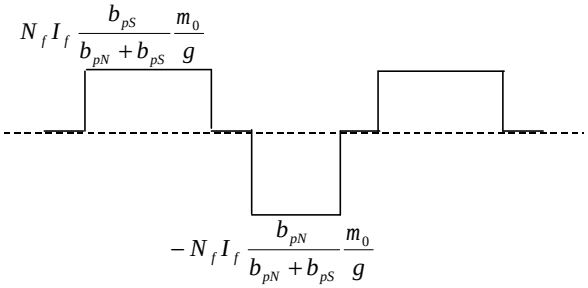

Fig. A.4.Lundell alternator field flux density waveform

The flux densities due to the north and south poles can be determined separately and added. The flux density contribution by the north poles can be expressed as

$$B_{rN} = \sum_{m=0}^{\infty} B_{rNm}\cos(mp(q-q_r)) \tag{A.16}$$

$$B_{rN0} = b_N\left(\frac{N_f I_f}{2}\frac{m_0}{g}\right)=\left(\frac{N_f I_f}{2}\right)\left(b_N\,\frac{m_0}{g}\right)= F_{rN}\Lambda_{N0} \tag{A.17}$$

$$B_{rNm} = \frac{2}{mp}\left(\frac{N_f I_f}{2}\frac{m_0}{g}\right)\sin(mb_N p) = \left(\frac{N_f I_f}{2}\right)\left(\frac{2}{mp}\frac{m_0}{g}\sin(mb_N p)\right)= F_{rN}\Lambda_{Nm} \tag{A.18}$$

$$b_N = \frac{\frac{z}{L}b_{p2}+\left(1-\frac{z}{L}\right)b_{p1}}{2t_p} \tag{A.19}$$

where b_{p2} and b_{p1} are the widths of the wider end and narrower end of a pole, respectively, and τ_p is a pole pitch. Similarly, the flux density waveforms due to the south poles are

$$B_{rS} = \sum_{m=0}^{\infty} B_{rSm}\cos(mp((q-p/p)-q_r)) \tag{A.20}$$

$$B_{rS0} = b_S\left(-\frac{N_f I_f}{2}\frac{m_0}{g}\right)=\left(-\frac{N_f I_f}{2}\right)\left(b_S\,\frac{m_0}{g}\right)= F_{rS}\Lambda_{S0} \tag{A.21}$$

$$B_{rSm} = \frac{2}{mp}\left(-\frac{N_f I_f}{2}\frac{m_0}{g}\right)\sin(mbp) \tag{A.22}$$

$$B_{rSm} = \left(-\frac{N_f I_f}{2}\right)\left(\frac{2}{mp}\frac{m_0}{g}\sin(mbp)\right)= F_{rS}\Lambda_{Sm}$$

$$b_S = \frac{\frac{z}{L}b_{p1}+\left(1-\frac{z}{L}\right)b_{p2}}{2t_p} \tag{A.23}$$

The sum of both waveforms gives the total flux density due to the field winding which are

$$B_r = B_{rN} + B_{rS}$$

$$B_r = \sum_{\substack{m=0\\ m\,\text{even}}}^{\infty}(B_{rNm} + B_{rSm})\cos(mp(q-q_r)) + \sum_{\substack{m=1\\ m\,\text{odd}}}^{\infty}(B_{rNm} - B_{rSm})\cos(mp(q-q_r)) \tag{A.24}$$

where the different harmonic components are

$$B_{r0} = \left(\frac{N_f I_f}{2}\right)(b_N - b_S)\frac{m_0}{g}\Big) \tag{A.25}$$

$$B_{rm} = \left(\frac{N_f I_f}{2}\right)\left(\frac{2}{mp}\frac{m_0}{g}(\sin(mb_N p)-\sin(mb_S p))\right)\cdot\cos(mp(q-q_r)) \qquad m\,\text{even} \tag{A.26}$$

$$B_{rm} = \left(\frac{N_f I_f}{2}\right)\left(\frac{2}{mp}\frac{m_0}{g}(\sin(mb_N p)+\sin(mb_S p))\right)\cdot\cos(mp(q-q_r)) \qquad m\,\text{odd} \tag{A.27}$$

d) Homopolar inductor alternator field flux density

For the inductor alternator, the flux density on one stack can be found to be as shown in Fig. A.5.

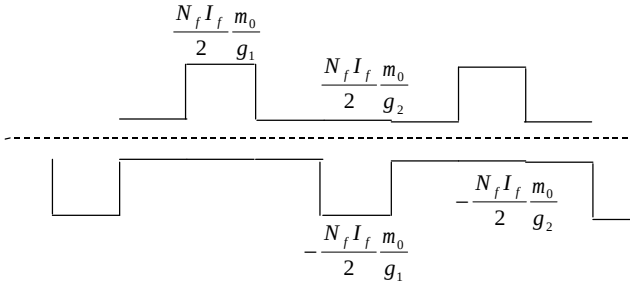

Fig. A.5. Homopolar inductor alternator field flux density waveform

The expression for the waveform in the air gap where the north poles are located are

$$B_{rN0} = F_{rN}\Lambda_{N0} = \left(\frac{N_f I_f}{2}\right)\left(b\left(\frac{m_0}{g_1}\right)+(1-b)\left(\frac{m_0}{g_2}\right)\right) \quad \text{(A.28)}$$

$$B_{rN0} = F_{rN}\Lambda_{N0} = \left(\frac{N_f I_f}{2}\right)\left(b\left(\frac{m_0}{g_1}\right)+(1-b)\left(\frac{m_0}{g_2}\right)\right) \quad \text{(A.29)}$$

$$B_{rNm} = F_{rN}\Lambda_{Nm} = \left(\frac{N_f I_f}{2}\right)\left(\frac{2}{mp}\left(\frac{m_0}{g_1}-\frac{m_0}{g_2}\right)\sin(mbp)\right) \quad \text{(A.30)}$$

where g_1 and g_2 are the shorter and longer air gap widths, respectively. Likewise, for the air gap where the south poles are, the flux density waveform due to the field winding can be shown to be

$$B_{rS} = \sum_{m=0}^{\infty} B_{rSm}\cos(mp((q-p/p)-q_r)) \quad \text{(A.31)}$$

$$B_{rS0} = F_{rS}\Lambda_{S0} = \left(-\frac{N_f I_f}{2}\right)\left(b\left(\frac{m_0}{g_1}\right)+(1-b)\left(\frac{m_0}{g_2}\right)\right) \quad \text{(A.32)}$$

$$B_{rSm} = F_{rS}\Lambda_{Sm} = \left(-\frac{N_f I_f}{2}\right)\left(\frac{2}{mp}\left(\frac{m_0}{g_1}-\frac{m_0}{g_2}\right)\sin(mbp)\right) \quad \text{(A.33)}$$

3) Armature flux densities

For the armature windings as sources of MMF, the MMF due to each winding is approximated as a square wave with a winding factor k_{wn}

$$F_a = \sum_{\substack{n=1 \\ n\text{odd}}}^{\infty} \frac{4}{np}\frac{N_s i_a}{2p}\frac{k_{wn}}{a}\cos(npq) \quad \text{(A.34)}$$

$$F_b = \sum_{\substack{n=1 \\ n\text{odd}}}^{\infty} \frac{4}{np}\frac{N_s i_b}{2p}\frac{k_{wn}}{a}\cos(n(pq-2p/3)) \quad \text{(A.35)}$$

$$F_c = \sum_{\substack{n=1 \\ n\text{odd}}}^{\infty} \frac{4}{np}\frac{N_s i_c}{2p}\frac{k_{wn}}{a}\cos(n(pq-4p/3)) \quad \text{(A.36)}$$

where N_s is the number of armature turns per phase. The combined MMF is

$$F_s = F_a + F_b + F_c$$

$$F_s = \sum_{n=1,7,\ldots,6k+1}^{\infty} \frac{3}{2}\frac{4}{np}\frac{N_s I_s}{2p}\frac{k_{wn}}{a}\sin(pq_r - f - npq) + \sum_{n=5,11,\ldots,6k-1}^{\infty} \frac{3}{2}\frac{4}{np}\frac{N_s I_s}{2p}\frac{k_{wn}}{a}\sin(pq_r - f + npq) \quad \text{(A.37)}$$

of which only the fundamental is considered. In order to determine the fundamental flux density in the air gap due to the three-phase armature currents, the fundamental MMF is multiplied by the 0th component and 2nd harmonic of the air gap permeance function. There are slight modifications though to the air gap as seen from the armature winding compared to that seen by the field winding. The non-salient wound-field alternator still has the same permeance. The salient-pole has a slight change. The interpolar gaps are no longer seen to be of infinite gap width. Also, the north and south poles need not be considered separate. The new permeance function assumes the following form

$$\Lambda' = \sum_{m=0}^{\infty}\Lambda'_m\cos(m(2p)(q-q_r)) \quad \text{(A.38)}$$

$$\Lambda'_o = b'\left(\frac{m_0}{g_1}\right)+(1-b')\left(\frac{m_0}{g_2}\right) \quad \text{(A.39)}$$

$$\Lambda'_m = \frac{2}{mp}\left(\frac{m_0}{g_1}-\frac{m_0}{g_2}\right)\sin(mb'p) \quad \text{(A.40)}$$

$$b' = b_p / t_p \quad \text{(A.41)}$$

$$\Lambda' \cong \Lambda'_0 + \Lambda'_1\cos(2p(q-q_r)) \quad \text{(A.42)}$$

For the Lundell alternator, the two permeance functions determined separately can be combined as one permeance function. For the north poles, the permeance function is

$$\Lambda_N = \sum_{m=0}^{\infty}\Lambda_{Nm}\cos(mp(q-q_r)) \quad \text{(A.43)}$$

$$\Lambda_{N0} = b_N\frac{m_0}{g} \quad \text{(A.44)}$$

$$\Lambda_{Nm} = \left(\frac{2}{mp}\frac{m_0}{g}\sin(mb_N p)\right) \quad \text{(A.45)}$$

For the south poles, the permeance function is

$$\Lambda_S = \sum_{m=0}^{\infty}\Lambda_{Sm}\cos(mp(q-q_r)) \quad \text{(A.46)}$$

$$\Lambda_{S0} = b_S\frac{m_0}{g} \quad \text{(A.47)}$$

$$\Lambda_{Sm} = \left(\frac{2}{mp}\frac{m_0}{g}\sin(mb_S p)\right) \quad \text{(A.48)}$$

The combined permeance function can be shown to be

$$\Lambda = \Lambda_N + \Lambda_S = \sum_{m=0}^{\infty}(\Lambda_{Nm}+\Lambda_{Sm})\cos(mp(q-q_r)) \quad \text{(A.49)}$$

$$\Lambda \cong (\Lambda_{N0} + \Lambda_{S0}) + (\Lambda_{N2} + \Lambda_{S2})\cos(2p(q - q_r)) \quad \text{(A.50)}$$

Likewise, for the homopolar inductor alternator, the permeance function is approximated as

$$\Lambda_N \cong \Lambda_{N0} + \Lambda_{N2}\cos(2p(q - q_r)) \quad \text{(A.51)}$$

for the north poles and

$$\Lambda_S \cong \Lambda_{S0} + \Lambda_{S2}\cos(2p(q - q_r)) \quad \text{(A.52)}$$

for the south poles. The flux density is then the fundamental component of the MMF multiplied by the approximate permeance function from which the fundamental component is obtained

$$B_{s1} = \left\{\left(F_{s1}\sin(p(q - q_r) - f)\right)\left(\Lambda_0 + \Lambda_2\cos(2p(q - q_r))\right)\right\}_1$$

$$B_{s1} = F_{s1}\left(\Lambda_0\sin(p(q - q_r) - f) - \frac{\Lambda_2}{2}\sin(p(q - q_r) + f)\right) \quad \text{(A.53)}$$

where the subscript 1 is used to represent the fundamental component.

4) Flux linkages

For the first three machines, the flux linked by the armature winding is

$$l = \frac{N_s k_w}{a}\int_0^L \int_{-p/2p}^{p/2p} B_1 R\, dq\, dz \quad \text{(A.54)}$$

For the inductor alternator, the flux linked is

$$l = \frac{N_s k_w}{a}\int_0^{L/2} \int_{-p/2p}^{p/2p} B_{N1} R\, dq\, dz + \frac{N_s k_w}{a}\int_{L'}^{L'+L/2} \int_{-p/2p}^{p/2p} B_{S1} R\, dq\, dz \quad \text{(A.55)}$$

which is the sum of the flux linked for the north and south poles separately. It can be shown that (A.54) and (A.55) are the same.

5) Lumped parameters

The field armature mutual inductance is

$$L_{af} = l_{af} / I_f \quad \text{(A.56)}$$

In order to determine the equivalent inductance and resistance due to armature reaction, the flux linked will end up having the following form

$$l_a = (L_x)I_s\sin(pq - f) - (L_y)I_s\sin((pq - f) + 2f) \quad \text{(A.57)}$$

seen earlier. From these L_s and R_s can both be determined since

$$L_s = L_x - L_y\cos(2f) \quad \text{(A.58)}$$

$$R_s = r_a + wL_y\sin(2f) \quad \text{(A.59)}$$

The lumped parameters for each alternator can then be derived.The non-salient wound-field synchronous alternator has the following lumped parameters:

$$l_a = \frac{N_s k_w}{a} RLF_{s1}\left(\frac{2}{p}\right)\left(\Lambda\sin(pq_r - f)\right) \quad \text{(A.60)}$$

$$L_{af} = \frac{N_s k_w}{a} RL\left(\frac{4}{p}\frac{N_f}{2p}k_{wf}\right)\left(\frac{m_0}{g}\right)\frac{2}{p}\cos(pq_r) \quad \text{(A.61)}$$

$$L_s = \frac{N_s k_w}{a} RL\left(\frac{3}{2}\frac{4}{p}\frac{N_s}{2p}\frac{k_w}{a}\right)\left(\frac{m_0}{g}\right)\frac{2}{p} \quad \text{(A.62)}$$

$$R_s = r_a \quad \text{(A.63)}$$

The salient wound-field synchronous alternator has the following lumped parameters:

$$l_{af} = \frac{N_s k_w}{a} RL(F_{rN} - F_{rS})\Lambda_1\left(\frac{2}{p}\cos(pq_r)\right) \quad \text{(A.64)}$$

$$l_a = \frac{N_s k_w}{a} RLF_{s1}\left(\frac{2}{p}\right)\left(\Lambda_0'\sin(pq_r - f) - \frac{\Lambda_1'}{2}\sin(pq_r + f)\right) \quad \text{(A.65)}$$

$$L_{af} = \frac{N_s k_w}{a} RL\left(2\frac{N_f}{2p}\right)\left(\frac{2}{p}\frac{m_0}{g}\sin\left(\frac{b_p p}{2t_p}\right)\right)\frac{2}{p}\cos(pq_r) \quad \text{(A.66)}$$

$$L_s = \frac{N_s k_w}{a} RL\left(\frac{3}{2}\frac{4}{p}\frac{N_s}{2p}\frac{k_w}{a}\right)\left(\frac{2}{p}\right)\left(\Lambda_0' - \frac{\Lambda_1'}{2}\cos(2f)\right)$$

$$L_s = \frac{N_s k_w}{a} RL\left(\frac{3}{2}\frac{4}{p}\frac{N_s}{2p}\frac{k_w}{a}\right)\left(\frac{2}{p}\right) \quad \text{(A.67)}$$

$$\cdot\left(\left(\frac{b_p}{t_p}\left(\frac{m_0}{g_1}\right) + \left(1 - \frac{b_p}{t_p}\right)\left(\frac{m_0}{g_2}\right)\right) - \frac{1}{2}\left(\frac{2}{p}\left(\frac{m_0}{g_1} - \frac{m_0}{g_2}\right)\sin\left(\frac{b_p p}{t_p}\right)\right)\cos(2f)\right)$$

$$R_s = r_a + w\frac{N_s k_w}{a} RL\left(\frac{3}{2}\frac{4}{p}\frac{N_s}{2p}\frac{k_w}{a}\right)\left(\frac{2}{p}\right)\left(\frac{\Lambda_1'}{2}\sin(2f)\right)$$

$$R_s = r_a + w\frac{N_s k_w}{a} RL\left(\frac{3}{2}\frac{4}{p}\frac{N_s}{2p}\frac{k_w}{a}\right)\left(\frac{2}{p}\right)$$

$$\cdot\left(\frac{1}{2}\left(\frac{2}{p}\left(\frac{m_0}{g_1} - \frac{m_0}{g_2}\right)\sin\left(\frac{b_p p}{t_p}\right)\right)\sin(2f)\right) \quad \text{(A.68)}$$

The Lundell alternator has the following lumped parameters:

$$L_{af} = \frac{8}{p}\frac{m_0 k_w N_f N_s RL}{pa\,(b_{p1}+b_{p2})\,g} \cdot \left(\begin{array}{l} \frac{b_{p1}+b_{p2}}{(b_{p2}-b_{p1})}\left(\cos\left(\frac{b_{p1}p}{2t_p}\right)-\cos\left(\frac{b_{p2}p}{2t_p}\right)\right) \\ -\frac{4t_p}{(b_{p2}-b_{p1})p}\left(\sin\left(\frac{b_{p2}p}{2t_p}\right)-\sin\left(\frac{b_{p1}p}{2t_p}\right)\right)\left(\frac{2}{p}\cos(pq_r)\right) \\ +\left(\cos\left(\frac{b_{p2}p}{2t_p}\right)+\cos\left(\frac{b_{p1}p}{2t_p}\right)\right) \end{array} \right) \quad \text{(A.69)}$$

$$l_a = \frac{N_s k_w}{a} RLF_{s1}\left(\frac{2}{p}\right) \cdot \left(\begin{array}{l} (\Lambda_{N0}+\Lambda_{S0})\sin(pq_r - f) \\ -\frac{1}{2}\left(\frac{2m_0}{2pg}\frac{2t_p}{(b_{p2}-b_{p1})p}\left(\cos\left(\frac{b_{p1}p}{t_p}\right)-\cos\left(\frac{b_{p2}p}{t_p}\right)\right)\right) \\ \cdot\sin(pq_r + f) \end{array} \right) \quad \text{(A.70)}$$

$$l_{af} = \frac{8}{p}\frac{m_0 k_w N_f I_f N_s RL}{pa\,(b_{p1}+b_{p2})\,g} \cdot \left(\begin{array}{l} \frac{b_{p1}+b_{p2}}{(b_{p2}-b_{p1})}\left(\cos\left(\frac{b_{p1}p}{2t_p}\right)-\cos\left(\frac{b_{p2}p}{2t_p}\right)\right) \\ -\frac{4t_p}{(b_{p2}-b_{p1})p}\left(\sin\left(\frac{b_{p2}p}{2t_p}\right)-\sin\left(\frac{b_{p1}p}{2t_p}\right)\right) \\ +\left(\cos\left(\frac{b_{p2}p}{2t_p}\right)+\cos\left(\frac{b_{p1}p}{2t_p}\right)\right) \end{array} \right) \cdot\left(\frac{2}{p}\cos(pq_r)\right) \quad \text{(A.71)}$$

$$L_s = \frac{N_s k_w}{a} RL\left(\frac{3}{2}\frac{4}{p}\frac{N_s}{2p}\frac{k_w}{a}\right)\left(\frac{2}{p}\right) \cdot \left(\begin{array}{l} \left(\frac{b_{p1}+b_{p2}}{2t_p}\frac{m_0}{g}\right) \\ -\frac{1}{2}\left(\frac{2m_0}{2pg}\frac{2t_p}{(b_{p2}-b_{p1})p}\left(\cos\left(\frac{b_{p1}p}{t_p}\right)-\cos\left(\frac{b_{p2}p}{t_p}\right)\right)\right)\cos(2f) \end{array} \right) \quad \text{(A.72)}$$

$$R_s = r_a + w\frac{N_s k_w}{a} RL\left(\frac{3}{2}\frac{4}{p}\frac{N_s}{2p}\frac{k_w}{a}\right)\left(\frac{2}{p}\right) \cdot \left(\begin{array}{l} \frac{1}{2}\left(\frac{2m_0}{2pg}\frac{2t_p}{(b_{p2}-b_{p1})p}\left(\cos\left(\frac{b_{p1}p}{t_p}\right)-\cos\left(\frac{b_{p2}p}{t_p}\right)\right)\right)\sin(2f) \end{array} \right) \quad \text{(A.73)}$$

And finally, the homopolar inductor alternator has the following lumped parameters:

$$l_{af} = \frac{N_s k_w}{a} RL\frac{(F_{rN}-F_{rS})}{2}\Lambda_{N1}\left(\frac{2}{p}\cos(pq_r)\right) \quad \text{(A.74)}$$

$$l_a = \frac{N_s k_w}{a} RLF_{s1}\left(\frac{2}{p}\right)\left(\Lambda_{N0}\sin(pq_r - f) - \frac{\Lambda_{N2}}{2}\sin(pq_r + f)\right) \quad \text{(A.75)}$$

$$L_{af} = \frac{N_s k_w}{a} RL\frac{\left(2\frac{N_f}{2}\right)\left(\frac{2}{p}\left(\frac{m_0}{g_1}-\frac{m_0}{g_2}\right)\sin\left(\frac{b_p p}{2t_p}\right)\right)}{2} \cdot\frac{2}{p}\cos(pq_r) \quad \text{(A.76)}$$

$$L_s = \frac{N_s k_w}{a} RL\left(\frac{3}{2}\frac{4}{p}\frac{N_s}{2p}\frac{k_w}{a}\right)\left(\frac{2}{p}\right)\left(\Lambda_{N0} - \frac{\Lambda_{N2}}{2}\cos(2f)\right)$$

$$L_s = \frac{N_s k_w}{a} RL\left(\frac{3}{2}\frac{4}{p}\frac{N_s}{2p}\frac{k_w}{a}\right)\left(\frac{2}{p}\right) \cdot \left(\begin{array}{l} \left(\frac{b_p}{2t_p}\left(\frac{m_0}{g_1}\right)+\left(1-\frac{b_p}{2t_p}\right)\left(\frac{m_0}{g_2}\right)\right) \\ -\frac{1}{2}\left(\frac{2}{2p}\left(\frac{m_0}{g_1}-\frac{m_0}{g_2}\right)\sin\left(\frac{b_p p}{t_p}\right)\right)\cos(2f) \end{array} \right) \quad \text{(A.77)}$$

$$R_s = r_a + w\frac{N_s k_w}{a} RL\left(\frac{3}{2}\frac{4}{p}\frac{N_s}{2p}\frac{k_w}{a}\right)\left(\frac{2}{p}\right)\left(\frac{\Lambda_{N2}}{2}\sin(2f)\right)$$

$$R_s = r_a + w\frac{N_s k_w}{a} RL\left(\frac{3}{2}\frac{4}{p}\frac{N_s}{2p}\frac{k_w}{a}\right)\left(\frac{2}{p}\right) \cdot\left(\frac{1}{2}\left(\frac{2}{2p}\left(\frac{m_0}{g_1}-\frac{m_0}{g_2}\right)\sin\left(\frac{b_p p}{t_p}\right)\right)\sin(2f)\right) \quad \text{(A.78)}$$

Note that the general forms of L_s and R_s from which L_{s0} and L_{s2} can be obtained are

$$L_s = \frac{N_s k_w}{a} RL\frac{F_{s1}}{I_s}\left(\frac{2}{p}\right)\left(\Lambda_0 - \frac{\Lambda_2}{2}\cos(2f)\right) \quad \text{(A.79)}$$

$$R_s = r_a + w\frac{N_s k_w}{a} RL\frac{F_{s1}}{I_s}\left(\frac{2}{p}\right)\left(\frac{\Lambda_2}{2}\cos(2f)\right) \quad \text{(A.80)}$$

6) Simplified lumped parameters

In order to obtain the simplified power comparisons in Section V, some simplifying assumptions were made. As can be found in Section V, equation (15), the power delivered to an impedance-matched load is based on the mutual inductance L_{af} and the synchronous inductance L_s. This section obtains these simplified inductances. For the non-salient wound field alternator, no simplifying assumptions are made and therefore (A.61) and (A.62) are used. For the salient wound field alternator, the pole width is assumed to be half a pole pitch ($b_p = t_p/2$), the larger air gap is ignored ($g_2 \to \infty$), and saliency is ignored ($\cos(2f)$ term). The simplified inductances are

$$L_{af} = \frac{N_s k_w}{a} RL\left(2\frac{N_f}{2p}\right)\left(\frac{2}{p}\frac{m_0}{g}\frac{1}{\sqrt{2}}\right)\frac{2}{p}\cos(pq_r) \qquad \text{(A.81)}$$

$$L_s = \frac{N_s k_w}{a} RL\left(\frac{3}{2}\frac{4}{p}\frac{N_s}{2p}\frac{k_w}{a}\right)\left(\frac{2}{p}\right)\left(\frac{1}{2}\left(\frac{m_0}{g_1}\right)\right) \qquad \text{(A.82)}$$

For the Lundell alternator, the poles are assumed to be rectangular and with widths equal to a pole pitch ($b_{p1} = b_{p2} = t_p$) . In addition, saliency is ignored. The simplified inductances are

$$L_{af} = \frac{8}{p}\frac{m_0 k_w N_f N_s RL}{pa(2t_p)g}(2t_p p)\left(\frac{2}{p}\cos(pq_r)\right) \qquad \text{(A.83)}$$

$$L_s = \frac{N_s k_w}{a} RL\left(\frac{3}{2}\frac{4}{p}\frac{N_s}{2p}\frac{k_w}{a}\right)\left(\frac{2}{p}\right)\left(\frac{m_0}{g}\right) \qquad \text{(A.84)}$$

For the homopolar inductor alternator, the width of a pole is made to span a pole pitch ($b_p = t_p$), and the larger air gap is ignored ($g_2 \to \infty$)

$$L_{af} = \frac{N_s k_w}{a} RL\frac{\left(2\frac{N_f}{2}\right)\left(\frac{2}{p}\left(\frac{m_0}{g_1}\right)\right)}{2}\frac{2}{p}\cos(pq_r) \qquad \text{(A.85)}$$

$$L_s = \frac{N_s k_w}{a} RL\left(\frac{3}{2}\frac{4}{p}\frac{N_s}{2p}\frac{k_w}{a}\right)\left(\frac{2}{p}\right)\left(\frac{1}{2}\left(\frac{m_0}{g_1}\right)\right) \qquad \text{(A.86)}$$

ACKNOWLEDGEMENT

We would like to acknowledge the support provided by the MIT/Industry Consortium on Advanced Electrical/Electronic Components and Systems.

REFERENCES

[1] D. J. Perreault, V. Caliskan, "Automotive Power Generation and Control", *IEEE Transactions on Power Electronics*, Vol. 19, No. 3, May 2004.

[2] C. P. Cho, D. R. Crecelius, "Vehicle Alternator/Generator Trends Toward Next Millenium," *Vehicle Electronics Conference*, Proceedings of the IEEE International, Vol. 1, Sept. 1999.

[3] V. Ostovic., J. M. Miller, V. K. Garg, R. D. Schultz, S. H. Swales, "A Magnetic Equivalent Circuit Based Performance Computation of a Lundell Alternator", *IEEE Transactions on Industry Applications*, Vol. 35, No. 4, July/August 1999.

[4] E. Richter, "New Developments in Very High Speed Electrical Alternators," *Intersociety Energy Conversion Engineering Conference*, 1971.

[5] K.G. Burger, H. P. Groter, H. J. Lutz, F. Meyer, W. Scheluter, "Alternators in Automotive Applications-State of the Art and Development Trends, "symposium "*Nebenaggregate im Fahrzeug*, Haus der Technik Essen, Oct. 5 and 6, 1994.

[6] J. A. N. Msekela, P. N. Materu, A. H. Nzali, "Development of a Homopolar Electrical Machine for High Power Density High Speed Applications", *African Electrical Technology Conference*, 1996.

[7] G. C. Jain, " Design Aspects of a Homopolar Inductor Alternator", *IEEE Transactions on Power Apparatus and Systems*, Vol. 83, pp. 1009-1015, October 1964.

[8] J. H. Walker, "The Theory of the Inductor Alternator", *Journal of IEE*, Vol. 89, pp. 227-241, 1942.

[9] N. Ellis, F. A. Collins, "Brushless Rotating Electrical Generators for Space Auxiliary Power Systems," *National Aeronautics and Space Administration*, Contract No. NAS 3-2783, Vol. 1, April 1965.

[10] G. A. Osborn, T. W. Salmon, "Application of the Electromagnetic Generator to Space Power Systems," *IEEE Transactions on Aerospace*, Vol. 2, No. 2, pp. 857-866, April 1964.

[11] L. G. Opel, "Design Features of Alternating Current Nadyne Generator," *IEEE Transactions on Aerospace*, Vol. 2, No. 2, pp. 888-895, April 1964.

[12] V. Caliskan, D.J. Perreault, T.M. Jahns, and J.G. Kassakian, "Analysis of Three-Phase Rectifier with Constant-Voltage Loads," *IEEE Transactions on Circuits and Systems-I: Fundamental Theory and Applications*, Vol. 50, No. 9, pp. 1120-1225, September 2003.